Numerical Study of Two-Species Chemotaxis Models*

Alexander Kurganov† and Mária Lukáčová-Medvid'ová‡

Abstract

We first conduct a comparative numerical study of two recently proposed two-species chemotaxis models. We show that different scenarios are possible: depending on the initial masses, either one or both cell densities may blow up, or a global solution may exist. In particular, our numerical results indicate answers on some open questions of possible blow up stated in [4, 7]. We then introduce two regularizations of the studied models and demonstrate that their solutions are capable of developing spiky structure without blowing up.

Key words: two-species chemotaxis models, second-order positivity preserving finite-volume method, finite-time blow-up.

AMS Subject Classification: 92C17, 76M12, 65M06, 35K55, 35B40.

1 Introduction

Chemotaxis is one of the most important mechanism in movement of biological species. It describes a collective movement of cells or biological species that is oriented towards the chemoattractant gradient. A classical PDE-based model of chemotaxis, the Patlak-Keller-Segel (PKS) system, was first proposed in [27] and [18, 19]. The classical PKS system as well as its more recent modifications (see, e.g., [2, 14, 16, 17, 28] and references therein) are capable of describing the aggregation of biological species and consequently a mechanism for self-organization of biological systems. In some of the above models, the cell aggregation may lead to a finite time blow-up of the solution provided the total initial cell mass is above a certain threshold (see [3, 11, 24]). However, the formation of singularities in the PKS model may be viewed as a purely mathematical artifact. Many regularized PKS-type systems admit global classical (yet spiky) solutions, which may better describe the biological aggregation phenomenon (as, e.g., in the regularized models studied in [2, 23, 26, 29, 33], see also a recent review [14]).

*Preprint AG Numerik, Institut für Mathematik, Oktober, 2011

†Mathematics Department, Tulane University, 6823 St. Charles Ave., New Orleans, LA 70118, USA and Institute of Mathematics, University of Mainz, Staudingerweg 9, 55099 Mainz, Germany; kurganov@math.tulane.edu

‡Institute of Mathematics, University of Mainz, Staudingerweg 9, 55099 Mainz, Germany; lukacova@uni-mainz.de

The aim of this paper is twofold. We first numerically investigate two models proposed and analytically studied in [4–9, 20, 34]. The first system reads

$$\begin{cases} (\rho_1)_t + \chi_1 \boldsymbol{\nabla} \cdot (\rho_1 \nabla c) = \mu_1 \Delta \rho_1, \\ (\rho_2)_t + \chi_2 \boldsymbol{\nabla} \cdot (\rho_2 \nabla c) = \mu_2 \Delta \rho_2, \qquad \boldsymbol{x} \in \Omega \subset \mathbb{R}^d, \ t > 0, \\ c_t = D \Delta c + \alpha_1 \rho_1 + \alpha_2 \rho_2 - \beta c, \end{cases} \tag{1.1}$$

where ρ_1 and ρ_2 denote the cell densities of the first and second species, respectively, and c is the concentration of the chemoattractant. The positive constants μ_i, χ_i, α_i $(i = 1, 2)$ and β are parameters of cell diffusion, chemotactic sensitivities, production and consumption rates, respectively. Finally, D is the chemoattractant diffusion coefficient. Throughout the paper we will assume that the second species has larger chemotactic sensitivity than the first one, that is,

$$\chi_1 < \chi_2.$$

Since the molecular diffusion is typically much faster than the cell diffusion, that is, both $\mu_1 \ll D$ and $\mu_2 \ll D$, the system (1.1) can be simplified by assuming that $\mu_i/D \approx 0$, $i = 1, 2$, which lead to the following system:

$$\begin{cases} (\rho_1)_t + \chi_1 \boldsymbol{\nabla} \cdot (\rho_1 \nabla c) = \mu_1 \Delta \rho_1, \\ (\rho_2)_t + \chi_2 \boldsymbol{\nabla} \cdot (\rho_2 \nabla c) = \mu_2 \Delta \rho_2, \qquad \boldsymbol{x} \in \Omega \subset \mathbb{R}^d, \ t > 0. \\ \Delta c + \gamma_1 \rho_1 + \gamma_2 \rho_2 - \zeta c = 0, \end{cases} \tag{1.2}$$

The models (1.1) and (1.2) can be viewed as direct extensions of the PKS system to the case of the chemotaxis motion of two noncompeting species that both consume and produce the same chemoattractant. As in the case of the classical PKS model, the main question we numerically investigate is: what are the conditions on initial masses and chemotactic parameters that determine whether the solution remain smooth and bounded or it blows up in a finite time? In the latter case, we would also like to determine whether the cell densities of both species blow up simultaneously or the cell density of the species with a larger chemosensitivity constant blows up first. These questions were first raised in [34] and further studied in [4, 5, 7]. More precisely, it has been proven analytically that depending on a particular set of parameter values and initial cell densities the solution may be globally regular or it may blow up within a finite time. However, in some cases, the theory fails to predict the behavior of the solution. Our numerical simulations indicate answers to some of these open questions.

The second main goal of our paper is to present and study two regularizations of (1.1). The first regularized system reads

$$\begin{cases} (\rho_1)_t + \boldsymbol{\nabla} \cdot (\rho_1 \boldsymbol{Q}_1(\chi_1 \nabla c)) = \mu_1 \Delta \rho_1, \\ (\rho_2)_t + \boldsymbol{\nabla} \cdot (\rho_2 \boldsymbol{Q}_2(\chi_2 \nabla c)) = \mu_2 \Delta \rho_2, \qquad \boldsymbol{x} \in \Omega \subset \mathbb{R}^d, \ t > 0, \\ c_t = D \Delta c + \alpha_1 \rho_1 + \alpha_2 \rho_2 - \beta c, \end{cases} \tag{1.3}$$

where the functions $\boldsymbol{Q}_1$ and $\boldsymbol{Q}_2$ are smooth saturated chemotactic fluxes $\boldsymbol{Q}_i(u_1, \ldots, u_d) = \boldsymbol{Q}_i(\boldsymbol{u}) = \big(Q_i^{(1)}(\boldsymbol{u}), \ldots, Q_i^{(d)}(\boldsymbol{u})\big)$ that satisfy the following properties:

$$\boldsymbol{Q}_i(\boldsymbol{0}) = \boldsymbol{0}, \quad |Q_i^{(j)}| \le C_i^j, \quad \frac{\partial Q_i^{(j)}}{\partial u_j} > 0 \ \ \forall \boldsymbol{u}, \ \ \forall i = 1, 2; j = 1, \ldots, d, \tag{1.4}$$

where C_i^j are constants. This regularization is similar to the one proposed in [2] for the PKS system. It is based on a fundamental biological property of the chemotactic flux—its boundedness (this feature is almost always lost in weakly nonlinear, small gradients expansions, underlying the derivation of most continuum models). The synthesized form of the saturated fluxes a function, which has the following universal features: It is linear at small gradients of c and is bounded at large gradients of c. There is a certain arbitrariness in the choice of the chemotactic flux functions $\boldsymbol{Q}_i$. A typical example of saturated chemotactic fluxes, which is used in all of our numerical experiments, is for $i = 1, 2$

$$\boldsymbol{Q}_i(\chi_i\nabla c) = \begin{cases} \chi_i\nabla c, & \text{if } \chi_i|\nabla c| \le s_i^*, \\ \left(\dfrac{\chi_i|\nabla c| - s_i^*}{\sqrt{1+(\chi_i|\nabla c| - s_i^*)^2}} + s_i^*\right)\dfrac{\nabla c}{|\nabla c|}, & \text{otherwise,} \end{cases} \tag{1.5}$$

where s_i^* are switching parameters, which define small gradient values, for which the system (1.3) reduces to the original system (1.1) (or (1.2)) so that the effect of saturated chemotactic flux is felt at large gradient regimes only. This is expected to result in solutions which are spiky but yet bounded for all times.

The second regularized system,

$$\begin{cases} (\rho_1)_t + \chi_1\boldsymbol{\nabla}\cdot\left(\dfrac{\rho_1}{1+\kappa\rho_1}\nabla c\right) = \mu_1\Delta\rho_1, \\ (\rho_2)_t + \chi_2\boldsymbol{\nabla}\cdot\left(\dfrac{\rho_2}{1+\kappa\rho_2}\nabla c\right) = \mu_2\Delta\rho_2, \qquad \boldsymbol{x}\in\Omega\subset\mathbb{R}^d,\ t>0, \\ c_t = D\Delta c + \alpha_1\rho_1 + \alpha_2\rho_2 - \beta c, \end{cases} \tag{1.6}$$

is similar to the density-dependent regularization from [31, 32]. Here, κ is a (small) regularization parameter and $\kappa \to 0$ leads to the original system (1.1). As in the single species case [13, 31], one expects a global classical solution of (1.6) to exist. At the same time, we will numerically demonstrate that the solutions of (1.6) typically have spiky structure and thus the system (1.6) can be used to model the aggregation phenomenon.

Throughout the paper, we will consider the systems (1.1), (1.2), (1.3) and (1.6) subject to the initial conditions $\rho_1(\boldsymbol{x}, 0) = \rho_1^0(\boldsymbol{x}) \ge 0$, $\rho_2(\boldsymbol{x}, 0) = \rho_2^0(\boldsymbol{x}) \ge 0$, $c(\boldsymbol{x}, 0) = c^0(\boldsymbol{x})$ and the homogeneous Neumann boundary conditions. These boundary conditions are zero-flux conditions for both the cell densities and chemoattractant concentration, which guarantee mass conservation.

The present paper will be organized as follows. In Section 2, we prove a-priori estimates for the regularized system (1.3). Section 3 is devoted to the description of the numerical method, which is a modification of the second-order positivity preserving upwind scheme from [1, 2]. Finally, Section 4 is devoted to the presentation and discussion of our numerical simulations.

2 L^∞ Bounds via Moser-Alikakos Iteration

Let us consider the original initial-boundary value problem (IBVP) for the system (1.3):

$$\begin{cases} (\rho_1)_t + \boldsymbol{\nabla}\cdot(\rho_1\boldsymbol{Q}_1(\chi_1\nabla c)) = \mu_1\Delta\rho_1, & \boldsymbol{x}\in\partial\Omega,\ t>0,\\ (\rho_2)_t + \boldsymbol{\nabla}\cdot(\rho_2\boldsymbol{Q}_2(\chi_2\nabla c)) = \mu_2\Delta\rho_2, & \boldsymbol{x}\in\partial\Omega,\ t>0,\\ c_t = D\Delta c + \alpha_1\rho_1 + \alpha_2\rho_2 - \beta c, & \boldsymbol{x}\in\partial\Omega,\ t>0,\\ \rho_i(\boldsymbol{x},0)=\rho_i^0(\boldsymbol{x}),\quad c(\boldsymbol{x},0)=c^0(\boldsymbol{x}), & \boldsymbol{x}\in\partial\Omega,\ i=1,2,\\ \dfrac{\partial\rho_1}{\partial\boldsymbol{n}} = \dfrac{\partial\rho_2}{\partial\boldsymbol{n}} = \dfrac{\partial c}{\partial\boldsymbol{n}} = 0, & \boldsymbol{x}\in\partial\Omega,\ t>0, \end{cases} \tag{2.1}$$

where $\partial\Omega$ is a Lipschitz continuous boundary with the outer normal $\boldsymbol{n}$.

In this section, we will prove a-priori estimates for positive solutions of (2.1). The following result is a generalization of analogous result for the one-species chemotaxis system from [2].

Theorem 2.1 *Let $(\rho_1(\boldsymbol{x},t),\rho_2(\boldsymbol{x},t),c(\boldsymbol{x},t))$ be a positive classical solution of the IBVP (2.1) with bounded nonnegative initial data. Then, for all $\boldsymbol{x}\in\bar\Omega$ and $t\ge 0$,*

$$\rho_1(\boldsymbol{x},t)\le C\left(1+\frac{C_1}{\mu_1}\right)^d \max\left\{\|\rho_1^0\|_{L^\infty(\Omega)},\|\rho_1^0\|_{L^1(\Omega)}\right\}, \tag{2.2}$$

$$\rho_2(\boldsymbol{x},t)\le C\left(1+\frac{C_2}{\mu_2}\right)^d \max\left\{\|\rho_2^0\|_{L^\infty(\Omega)},\|\rho_2^0\|_{L^1(\Omega)}\right\}, \tag{2.3}$$

$$\begin{aligned} c(\boldsymbol{x},t)&\le \|c^0\|_{L^\infty(\Omega)}\\ &\quad + C\left(\frac{\beta}{\alpha_1}\left(1+\frac{C_1}{\mu_1}\right)^d + \frac{\beta}{\alpha_2}\left(1+\frac{C_2}{\mu_2}\right)^d\right)\max_{i=1,2}\left\{\|\rho_i^0\|_{L^\infty(\Omega)},\|\rho_i^0\|_{L^1(\Omega)}\right\}, \end{aligned} \tag{2.4}$$

where $C=C(d,\Omega)$ is a constant, which depends on d and Ω only, and $C_i=\max_j C_i^{(j)}$, $i=1,2$.

Proof: We begin by multiplying the density equations in (2.1) by ρ_1^{s-1} and ρ_2^{s-1} ($s\ge 2$), respectively. Then, integrating by parts, applying the chain rule, using the boundedness of $|\boldsymbol{Q}_i|$ and the inequality (see [2, 21])

$$\|u\|^2_{L^2(\Omega)}\le\varepsilon\|\nabla u\|^2_{L^2(\Omega)} + K\left(1+\varepsilon^{-\frac{d}{2}}\right)\|u\|^2_{L^1(\Omega)} \tag{2.5}$$

with a suitable ε yields the following estimates:

$$\begin{aligned} \frac{1}{s}\frac{d}{dt}\int\limits_\Omega \rho_i^s\,d\boldsymbol{x} &= -\mu_i\int\limits_\Omega \nabla\rho_i\cdot\nabla\left(\rho_i^{s-1}\right)\,d\boldsymbol{x} + \int\limits_\Omega \rho_i\boldsymbol{Q}_i(\chi_i\nabla c)\cdot\nabla\left(\rho_i^{s-1}\right)\,d\boldsymbol{x}\\ &\le -\frac{4\mu_i(s-1)}{s^2}\int\limits_\Omega\left|\nabla\left(\rho_i^{\frac{s}{2}}\right)\right|^2\,d\boldsymbol{x} + \frac{2C_i(s-1)}{s}\int\limits_\Omega\rho_i^{\frac{s}{2}}\left|\nabla\left(\rho_i^{\frac{s}{2}}\right)\right|\,d\boldsymbol{x}\\ &\le -\frac{4\mu_i(s-1)}{s^2}\int\limits_\Omega\left|\nabla\left(\rho_i^{\frac{s}{2}}\right)\right|^2\,d\boldsymbol{x} + \frac{C_i(s-1)}{s}\int\limits_\Omega\left(\frac{2\mu_i}{C_is}\left|\nabla\left(\rho_i^{\frac{s}{2}}\right)\right|^2+\frac{C_is}{2\mu_i}\rho_i^s\right)d\boldsymbol{x}\\ &\le -\frac{2\mu_i(s-1)}{s^2}\int\limits_\Omega\left|\nabla\left(\rho_i^{\frac{s}{2}}\right)\right|^2\,d\boldsymbol{x} + \frac{C_i^2(s-1)}{2\mu_i}\int\limits_\Omega\rho_i^s\,d\boldsymbol{x},\quad i=1,2. \end{aligned} \tag{2.6}$$

The last term in (2.6) is estimated using the inequality (2.5) with $u = \rho_i^{\frac{s}{2}}$ and ε such that $\frac{C_i^2(s-1)}{2\mu_i} = \frac{2\mu_i(s-1)}{s^2\varepsilon} - \frac{C_i^2(s-1)}{2\mu_i} \iff \varepsilon = 2(\frac{\mu_i}{C_i s})^2$.

This results in

$$\begin{aligned}\frac{C_i^2(s-1)}{2\mu_i}\int_\Omega \rho_i^s\,d\boldsymbol{x} &= \frac{2\mu_i(s-1)}{s^2\varepsilon}\int_\Omega \rho_i^s\,d\boldsymbol{x} - \frac{C_i^2(s-1)}{2\mu_i}\int_\Omega \rho_i^s\,d\boldsymbol{x}\\ &\le \frac{2\mu_i(s-1)}{s^2}\left\|\nabla\left(\rho_i^{\frac{s}{2}}\right)\right\|^2_{L^2(\Omega)} + \frac{2\mu_i(s-1)K(1+\varepsilon^{-\frac{d}{2}})}{s^2\varepsilon}\left\|\rho_i^{\frac{s}{2}}\right\|^2_{L^1(\Omega)} - \frac{C_i^2(s-1)}{2\mu_i}\int_\Omega \rho_i^s\,d\boldsymbol{x}.\end{aligned} \tag{2.7}$$

Substituting (2.7) into (2.6), we obtain

$$\frac{d}{dt}\int_\Omega \rho_i^s\,d\boldsymbol{x} \le -\frac{C_i^2 s(s-1)}{2\mu_i}\int_\Omega \rho_i^s\,d\boldsymbol{x} + \frac{C_i^2 s(s-1)K\left(1+\left(\frac{sC_i}{\sqrt{2}\mu_i}\right)^d\right)}{\mu_i}\left(\int_\Omega \rho_i^{\frac{s}{2}}\,d\boldsymbol{x}\right)^2.$$

We then fix $T \in (0,\infty)$, multiply both sides of the last inequality by the integrating factor $e^{\kappa t}$, where $\kappa := C_i^2 s(s-1)/(2\mu_i)$, and integrate over the time interval $[0,t]$ for $t \in [0,T]$ to obtain

$$\int_\Omega \rho_i^s(\boldsymbol{x},t)\,d\boldsymbol{x} \le \int_\Omega (\rho_i^0)^s(\boldsymbol{x})\,d\boldsymbol{x} + 2K\left(1+\frac{sC_i}{\mu_i}\right)^d \sup_{0\le t\le T}\left(\int_\Omega \rho_i^{\frac{s}{2}}(\boldsymbol{x},t)\,d\boldsymbol{x}\right)^2. \tag{2.8}$$

Let us now define the function

$$M_i(s) := \max\left\{\|\rho_i^0\|_{L^\infty(\Omega)}, \sup_{0\le t\le T}\left(\int_\Omega \rho_i^s\,d\boldsymbol{x}\right)^{\frac{1}{s}}\right\}, \tag{2.9}$$

which satisfies (from (2.8)):

$$M_i(s) \le \left(\widetilde{K}\left(1+\frac{sC_i}{\mu_i}\right)^d\right)^{\frac{1}{s}} M_i(s/2), \quad \forall s \ge 2,$$

where the constant $\widetilde{K}$ depends on d and Ω only. Taking $s = 2^k,\ k = 1,2,\ldots$ and applying the above inequality recursively we obtain

$$M_i(2^k) \le C(1+C_i\mu_i)^d M_i(1),$$

where $C = C(d,\Omega)$. Now letting $k \to \infty$, we conclude that

$$\|\rho_i(\cdot,t)\|_{L^\infty(\Omega)} \le C\left(1+\frac{C_i}{\mu_i}\right)^d M_i(1), \quad \forall t \ge 0. \tag{2.10}$$

Finally, we note the total mass of the cells remains constant in time (this can be verified by integrating the density equations in (2.1) over Ω), and therefore

$$M_i(1) = \max\left\{\|\rho_i^0\|_{L^\infty(\Omega)}, \|\rho_i^0\|_{L^1(\Omega)}\right\}, \quad i = 1,2, \tag{2.11}$$

and the estimate (2.2) for the cell densities $\rho_i(\boldsymbol{x},t)$ follows from (2.10), (2.11).

Let us denote by $M(1):=\max_{i=1,2}\left(M_1(1),M_2(1)\right)$. In order to obtain a bound on chemoattractant concentration $c(\boldsymbol{x},t)$, we compare it with the solution of the following initial value problem (IVP):

$$\begin{cases}\dfrac{dw}{dt}=-\beta w+C\left(\alpha_1\left(1+\dfrac{C_1}{\mu_1}\right)^d+\alpha_2\left(1+\dfrac{C_1}{\mu_1}\right)^d\right)M(1),\\ w(0)=\|c^0\|_{L^\infty(\Omega)}.\end{cases}$$

The comparison principle then yields

$$\begin{aligned}0\le c(\boldsymbol{x},t)\le w(t)&=\mathrm{e}^{-\beta t}\|c^0\|_{L^\infty(\Omega)}+C\left(1-\mathrm{e}^{-\beta t}\right)\left(\frac{\alpha_1}{\beta}\left(1+\frac{C_i}{\mu_i}\right)^d+\frac{\alpha_1}{\beta}\left(1+\frac{C_i}{\mu_i}\right)^d\right)M(1)\\ &\le\|c^0\|_{L^\infty(\Omega)}+C\left(\frac{\alpha_1}{\beta}\left(1+\frac{C_1}{\mu_1}\right)^d+\frac{\alpha_2}{\beta}\left(1+\frac{C_2}{\mu_2}\right)^d\right)\max_{i=1,2}\left\{\|\rho_i^0\|_{L^\infty(\Omega)}\|\rho_i^0\|_{L^1(\Omega)}\right\},\end{aligned}\tag{2.12}$$

which completes the proof of Theorem 2.1. ■

Remark 2.1 An alternative L^∞ bounds on ρ_1 and ρ_2 can be obtained using the results from [15]. However, the estimates (2.2) and (2.3) explicitly show the dependence of the bounds on the number of dimensions d and the viscosity coefficients μ_1 and μ_2.

Remark 2.2 Note that using the L^∞-bounds established in Theorem 2.1, parabolic boundary L^p-estimates and Schauder estimates (see, e.g., [21]), one can obtain that $(\rho_1)_t,(\rho_2)_t,c_t$ and all spatial partial derivatives of ρ_1, ρ_2 and c up to order two are bounded on $\bar{\Omega}\times[0,\infty)$. This will lead to a global existence result similar to the one established in [2] for the one-species chemotaxis system. As it has been illustrated by our numerical experiments (shown in Section 4), the regularized solution while being bounded for all times, may develop spiky (even multi-spiky) structures that model aggregation phenomena.

3 Numerical Scheme

The numerical results presented in this paper are obtained using a second-order positivity preserving upwind scheme, which is a rather straightforward extension of the hybrid finite-volume-finite-difference scheme developed in [1,2] for the single species chemotaxis models. In this section, we briefly describe the scheme for the two-species chemotaxis system

$$\begin{cases}(\rho_1)_t+\nabla\cdot\big(g(\rho_1)\boldsymbol{Q}_1(\chi_1\nabla c)\big)=\mu_1\Delta\rho_1,\\ (\rho_2)_t+\nabla\cdot\big(g(\rho_2)\boldsymbol{Q}_2(\chi_2\nabla c)\big)=\mu_2\Delta\rho_2,\\ \varepsilon c_t=D\Delta c+\alpha_1\rho_1+\alpha_2\rho_2-\beta c,\end{cases}\tag{3.1}$$

where $\varepsilon=0$ or $\varepsilon=1$ and the functions g, Q_1 and Q_2 may be either linear or nonlinear so that the system (3.1) reduces to either (1.1), (1.2), (1.3) or (1.6).

We introduce a Cartesian mesh consisting of the uniform cells $C_{j,k}=[x_{j-\frac12},x_{j+\frac12}]\times[y_{k-\frac12},y_{k+\frac12}]$ of the size $\Delta x\Delta y$ centered at (x_j,y_k). The computed quantities are the cell averages of cell densities

ρ_i,

$$(\bar{\rho}_i)_{j,k}(t) \approx \frac{1}{\Delta x\Delta y}\iint\limits_{C_{j,k}} \rho_i(x,y,t)\,dxdy,$$

and the point values of the chemoattractant concentration c, $c_{j,k}(t) \approx c(x_j, y_k, t)$, which are evolved in time according to the semi-discrete scheme:

$$\begin{cases} \dfrac{d(\bar{\rho}_i)_{j,k}}{dt} = -\dfrac{(H_i)^x_{j+\frac12,k} - (H_i)^x_{j-\frac12,k}}{\Delta x} - \dfrac{(H_i)^y_{j,k+\frac12} - (H_i)^y_{j,k-\frac12}}{\Delta y} \\ \qquad\qquad + \mu_i\left(\dfrac{(\bar{\rho}_i)_{j-1,k} - 2(\bar{\rho}_i)_{j,k} + (\bar{\rho}_i)_{j+1,k}}{(\Delta x)^2} + \dfrac{(\bar{\rho}_i)_{j,k-1} - 2(\bar{\rho}_i)_{j,k} + (\bar{\rho}_i)_{j,k+1}}{(\Delta y)^2}\right),\ i=1,2, \\ \varepsilon\dfrac{dc_{j,k}}{dt} = D\left(\dfrac{c_{j-1,k} - 2c_{j,k} + c_{j+1,k}}{(\Delta x)^2} + \dfrac{c_{j,k-1} - 2c_{j,k} + c_{j,k+1}}{(\Delta y)^2}\right) + \alpha_1(\bar{\rho}_1)_{j,k} + \alpha_2(\bar{\rho}_2)_{j,k} - \beta c_{j,k}. \end{cases} \tag{3.2}$$

Here, $(H_i)^x_{j+\frac12,k}$ and $(H_i)^y_{j,k+\frac12}$ are the following upwind numerical fluxes:

$$(H_i)^x_{j+\frac12,k} = (g_i)_{j+\frac12,k}\,Q_i^{(1)}\left(\chi_i\,\frac{c_{j+1,k} - c_{j,k}}{\Delta x}\right), \quad (H_i)^y_{j,k+\frac12} = (g_i)_{j,k+\frac12}\,Q_i^{(2)}\left(\chi_i\,\frac{c_{j,k+1} - c_{j,k}}{\Delta y}\right), \tag{3.3}$$

where $Q_i^{(1)}$ and $Q_i^{(2)}$ are the components of the vector function $\boldsymbol{Q}_i$ (see (1.4)) and

$$(g_i)_{j+\frac12,k} = \begin{cases} g\big((\rho_i)^{\rm E}_{j,k}\big), & \text{if } \ Q_i^{(1)}\left(\chi_i\,\dfrac{c_{j+1,k} - c_{j,k}}{\Delta x}\right) > 0, \\ g\big((\rho_i)^{\rm W}_{j+1,k}\big), & \text{otherwise,} \end{cases}$$

$$(g_i)_{j,k+\frac12} = \begin{cases} g\big((\rho_i)^{\rm N}_{j,k}\big), & \text{if } \ Q_i^{(2)}\left(\chi_i\,\dfrac{c_{j,k+1} - c_{j,k}}{\Delta y}\right) > 0, \\ g\big((\rho_i)^{\rm S}_{j,k+1}\big), & \text{otherwise.} \end{cases}$$

The point values $(\rho_i)^{\rm E\,(W,N,S)}_{j,k}$ are obtained using the piecewise linear reconstruction

$$(\widetilde{\rho}_i)(x,y) = (\bar{\rho}_i)_{j,k} + ((\rho_i)_x)_{j,k}(x - x_j) + ((\rho_i)_y)_{j,k}(y - y_k), \qquad (x,y) \in C_{j,k},$$

with the slopes $((\rho_i)_x)_{j,k}$ and $((\rho_i)_y)_{j,k}$ calculated using the minmod2 limiter (see, e.g., [22,25,30]):

$$((\rho_i)_x)_{j,k} = \text{minmod}\left(2\,\frac{(\bar{\rho}_i)_{j+1,k} - (\bar{\rho}_i)_{j,k}}{\Delta x},\ \frac{(\bar{\rho}_i)_{j+1,k} - (\bar{\rho}_i)_{j-1,k}}{2\Delta x},\ 2\,\frac{(\bar{\rho}_i)_{j,k} - (\bar{\rho}_i)_{j-1,k}}{\Delta x}\right),$$

$$((\rho_i)_y)_{j,k} = \text{minmod}\left(2\,\frac{(\bar{\rho}_i)_{j,k+1} - (\bar{\rho}_i)_{j,k}}{\Delta y},\ \frac{(\bar{\rho}_i)_{j,k+1} - (\bar{\rho}_i)_{j,k-1}}{2\Delta y},\ 2\,\frac{(\bar{\rho}_i)_{j,k} - (\bar{\rho}_i)_{j,k-1}}{\Delta y}\right),$$

where the minmod function is defined by

$$\text{minmod}(z_1, z_2, \ldots, z_m) := \begin{cases} \min(z_1, z_2, \ldots, z_m), & \text{if } \ z_\ell > 0 \ \ \forall \ell = 1, \ldots, m, \\ \max(z_1, z_2, \ldots, z_m), & \text{if } \ z_\ell < 0 \ \ \forall \ell = 1, \ldots, m, \\ 0, & \text{otherwise.} \end{cases}$$

Thus, we have for $i = 1, 2$

$$(\rho_i)^{\rm E}_{j,k} = (\widetilde{\rho}_i)(x_{j+\frac12}, y_k),\ (\rho_i)^{\rm W}_{j,k} = (\widetilde{\rho}_i)(x_{j-\frac12}, y_k),\ (\rho_i)^{\rm N}_{j,k} = (\widetilde{\rho}_i)(x_j, y_{k+\frac12}),\ (\rho_i)^{\rm S}_{j,k} = (\widetilde{\rho}_i)(x_j, y_{k-\frac12}).$$

Remark 3.1 Notice that in the above formulae, the quantities $(\bar{\rho}_i)_{j,k}$, $c_{j,k}$, $(H_i)^x_{j+\frac{1}{2},k}$, $(H_i)^y_{j,k+\frac{1}{2}}$, $(\rho_i)_{j+\frac{1}{2},k}$, $(\rho_i)_{j,k+\frac{1}{2}}$, $(\rho_i)^{\mathrm{E\,(W,N,S)}}_{j,k}$, $((\rho_i)_x)_{j,k}$, $((\rho_i)_y)_{j,k}$ and the functions $(\widetilde{\rho}_i)(x,y)$, $i=1,2$ depend on time, but we suppress this dependence for brevity.

If $\varepsilon=1$, then the semi-discrete scheme (3.2) is a system of time-dependent ODEs, which has to be integrated numerically using a stable and accurate ODE solver. In this paper, we have used the third-order strong stability preserving (SSP) Runge-Kutta method from [10]. The efficiency of the fully discrete method can be improved by applying an SSP implicit-explicit Runge-Kutta method (see, e.g., [12] and references therein), as discussed in [1].

If $\varepsilon=0$, then the last equation in (3.1) becomes an elliptic equation for c, and consequently the last equation in (3.2) becomes a system of linear algebraic equations. This system has to be solved using a proper linear algebra solver. One time step of the resulting algorithm will then consist of an explicit time advance of ρ_1 and ρ_2 followed by solving the last equation in (3.2) for c using the values of ρ_1 and ρ_2 from the new time level.

4 Numerical Experiments

In this section, we present the results of our numerical experiments that clarify the behavior of the solutions of the studied two-species chemotaxis systems in two space dimensions. We restrict our consideration to the two-dimensional (2-D) case since the theoretical results/open questions in [4, 5, 7] were obtained/formulated for the 2-D version of the system (1.2).

In all of the examples below, we take $\alpha_1=\alpha_2=\beta=\gamma_1=\gamma_2=\zeta=1$.

4.1 Parabolic-Elliptic Systems

We first consider the parabolic-elliptic system (1.2) and its regularization with a bounded chemotaxis fluxes (with $\boldsymbol{Q}_1$ and $\boldsymbol{Q}_2$ satisfying (1.4)):

$$\begin{cases} (\rho_1)_t+\boldsymbol{\nabla}\cdot(\rho_1\boldsymbol{Q}_1(\chi_1\nabla c))=\mu_1\Delta\rho_1,\\ (\rho_2)_t+\boldsymbol{\nabla}\cdot(\rho_2\boldsymbol{Q}_2(\chi_2\nabla c))=\mu_2\Delta\rho_2,\\ \Delta c+\gamma_1\rho_1+\gamma_2\rho_2-\zeta c=0. \end{cases} \tag{4.1}$$

Without loss of generality we set $\mu_2=1$. We denote by θ_1 and θ_2 the initial masses

$$\theta_1:=\int\limits_\Omega \rho_1(\boldsymbol{x},t)\,d\boldsymbol{x}=\int\limits_\Omega \rho_1^0(\boldsymbol{x})\,d\boldsymbol{x},\quad \theta_2:=\int\limits_\Omega \rho_2(\boldsymbol{x},t)\,d\boldsymbol{x}=\int\limits_\Omega \rho_2^0(\boldsymbol{x})\,d\boldsymbol{x}.$$

Following [4, 7], we split the (θ_1, θ_2)-plane into the following four regions, outlined in Figure 4.1:

- Region **A**: $\dfrac{8\pi\mu_1\theta_1}{\chi_1} + \dfrac{8\pi\theta_2}{\chi_2} - (\theta_1+\theta_2)^2 \geq 0$ and $\theta_2 \leq \dfrac{8\pi}{\chi_2}$;
- Region **B**: $\dfrac{8\pi\mu_1\theta_1}{\chi_1} + \dfrac{8\pi\theta_2}{\chi_2} - (\theta_1+\theta_2)^2 \geq 0$ and $\theta_2 \geq \dfrac{8\pi}{\chi_2}$;
- Region **C**: $\theta_1+\theta_2 \leq \dfrac{8\pi}{\chi_1}$ and $\dfrac{8\pi\mu_1\theta_1}{\chi_1} + \dfrac{8\pi\theta_2}{\chi_2} - (\theta_1+\theta_2)^2 \leq 0$;
- Region **D**: $\theta_1+\theta_2 > \dfrac{8\pi}{\chi_1}$.

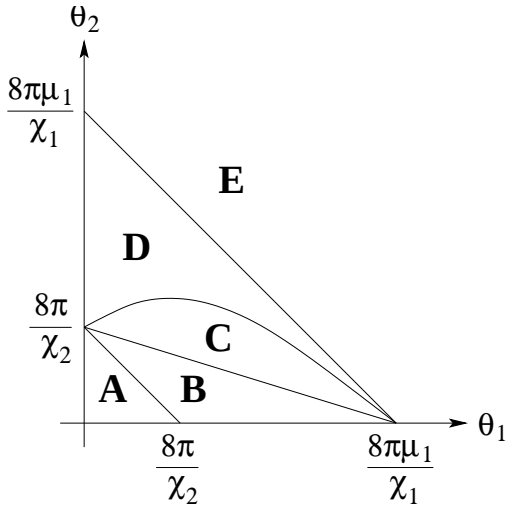

Figure 4.1: Four different regions in the (θ_1, θ_2)-plane.

In [4, 7], the following results were proved for the 2-D IVP for the parabolic-elliptic system (1.2) with $\gamma_1 = \gamma_2 = \zeta = \mu_2 = 1$:

- There is a global classical solution in Region **A** (the proof is based on the energy functions that provide a-priori estimates for the entropy of (1.2));
- In Region **C**, ρ_2 blows up faster than ρ_1;
- In Region **D**, ρ_1 and ρ_2 blow up at the same rate.

The question on the solution behavior in Region **B** remains open and we investigate it numerically. We study the systems (1.2) and (4.1) on a large square domain (either $[-1.5, 1.5]\times[-1.5, 1.5]$ or $[-3, 3] \times [-3, 3]$) and use the Neumann boundary conditions, which are typically used to represent open boundary conditions on truncated computational domains. In none of the numerical examples reported below, the solution behavior was affected by the boundary conditions, that is, all of the numerical solutions remain flat near the boundaries. This makes us to believe that the solution in $\mathbb{R}^2$ should behave similarly.

4.1.1 The Original System (1.2)

Example 1: Global Existence in Region A. We first consider the system (1.2) with $\chi_1 = 1$, $\chi_2 = 10$, $\mu_1 = 1$, and subject to the following initial data:

$$\rho_1(x,y,0) \equiv \rho_2(x,y,0) = 50\, e^{-100(x^2+y^2)}. \tag{4.2}$$

As one can see in Figure 4.2, the magnitude of both ρ_1 and ρ_2 decays and the solution remains smooth and bounded.

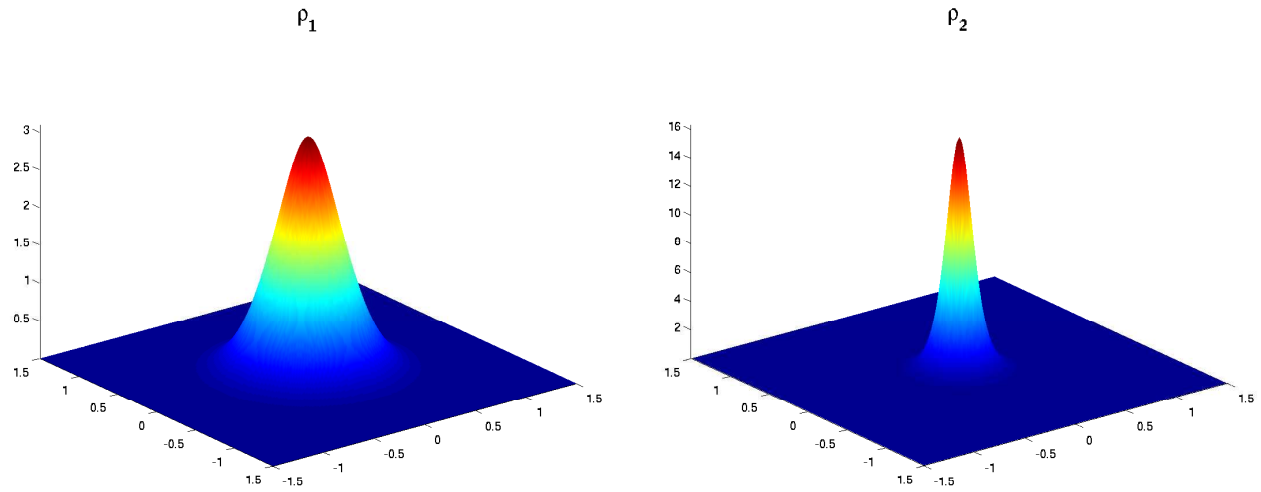

Figure 4.2: Example 1: ρ_1 and ρ_2 at time $t = 0.05$, computed on the 200×200 uniform mesh.

Example 2: Different Types of Blow-Up of ρ_1 and ρ_2 in Region B. We now consider the system (1.2) with $\chi_1 = 1$, $\chi_2 = 20$, $\mu_1 = 1$, and subject to the same, radially symmetric initial data (4.2). Figure 4.3 suggests that ρ_2 blows up while ρ_1 remains bounded. Moreover, the magnitude of ρ_1 seems to decay in time.

However, this would contradict the analytical results on simultaneous blow-up in Region **B** proved in [5,7] for radially symmetric initial data. We therefore perform a mesh refinement study to carefully monitor the behavior of $\max_\Omega \rho_1(x,y,0.05)$ and $\max_\Omega \rho_2(x,y,0.05)$ as a function of N, where the computational grid is $N \times N$. The dependence of $\max_\Omega \rho_1(x,y,0.05)$ on N together with the algebraic function $\xi_1(N) = 1.266(2N+10)^{1/4}$ are shown in Figure 4.4 (left). This results indicate that ρ_1 still blows up, but does not develop a δ-type singularity and therefore its blow-up is extremely hard to verify numerically.

In contrast, ρ_2 collapses to a δ-function as indicated in Figure 4.4 (right), where we plot $\max_\Omega \rho_2(x,y,0.05)$ as a function of N together with the quadratic function $\xi_2(N) = 0.0266(N-8)^2$. Note that this quadratic increase indeed reflects a δ-type singularity since using either a finite-volume, finite-difference or finite-element method 2-D δ-functions can only be resolved so that

$$\max_{j,k}(\rho_2)_{j,k} \sim \frac{1}{\Delta x \Delta y}.$$

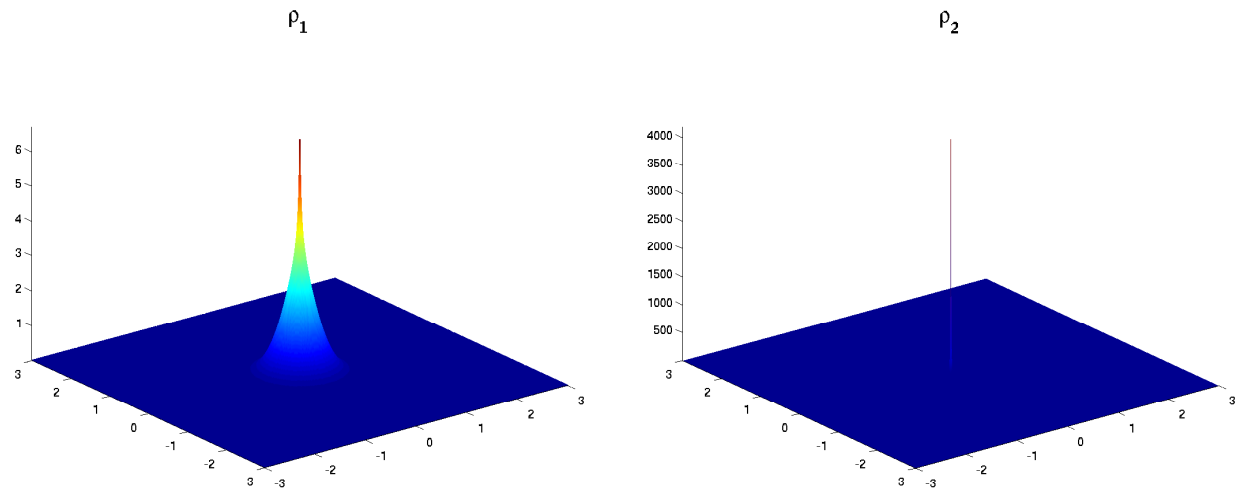

Figure 4.3: Example 2: ρ_1 and ρ_2 at time $t = 0.05$, computed on the 400×400 uniform mesh.

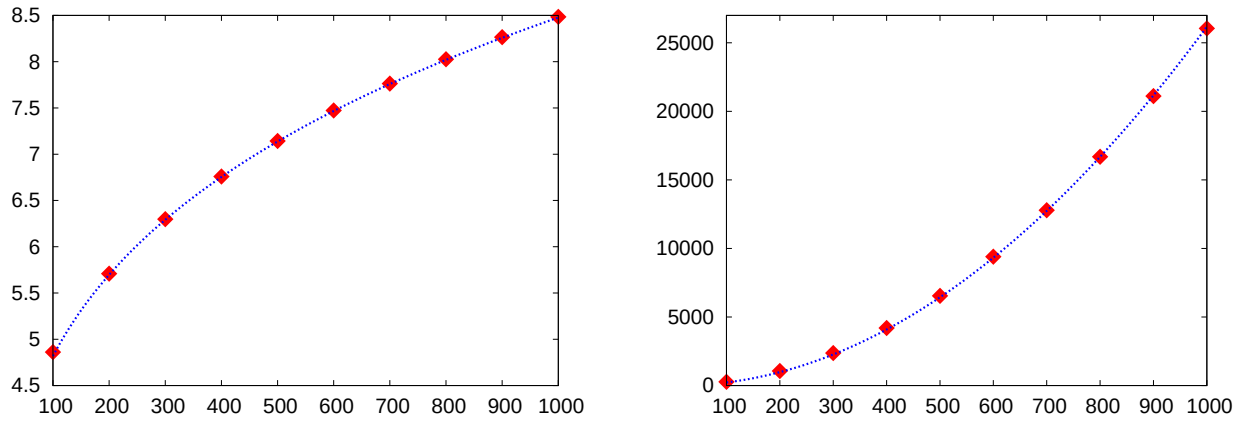

Figure 4.4: Example 2: $\max\limits_{(x,y)\in\Omega} \rho_1(x, y, 0.05)$ together with $\xi_1(N) = 1.266(2N + 10)^{1/4}$ (left) and $\max\limits_{(x,y)\in\Omega} \rho_2(x, y, 0.05)$ together with $\xi_2(N) = 0.0266(N - 8)^2$ (right) as functions of N.

Example 3: Blow-Up of ρ_1 and ρ_2 with Non-Radial Initial Data in Region B. The theoretical blow-up results for Region **B** reported in [5,7] only apply to radially symmetric initial data. However, behavior of solutions with non-radially symmetric initial data is still an open problem. In order to numerically investigate this case we take the following initial data:

$$\rho_1(x, y, 0) = 12.5\, e^{-100(x^2/16+y^2)}, \quad \rho_2(x, y, 0) = 12.5\, e^{-100(x^2+y^2/16)}, \tag{4.3}$$

and numerically solve the IVP (1.2), (4.3) with $\chi_1 = 1$, $\chi_2 = 20$ and $\mu_1 = 1$ in the domain $\Omega = [-3, 3] \times [-3, 3]$. The results obtained using a uniform 400×400 mesh are shown in Figure 4.5. They are quite similar to the corresponding results obtained in the radially symmetric case, see Figure 4.3.

To better understand the difference in the behavior of ρ_1 and ρ_2, we perform a mesh refinement study similar to the one conducted in Example 2. The results shown in Figure 4.6 support the

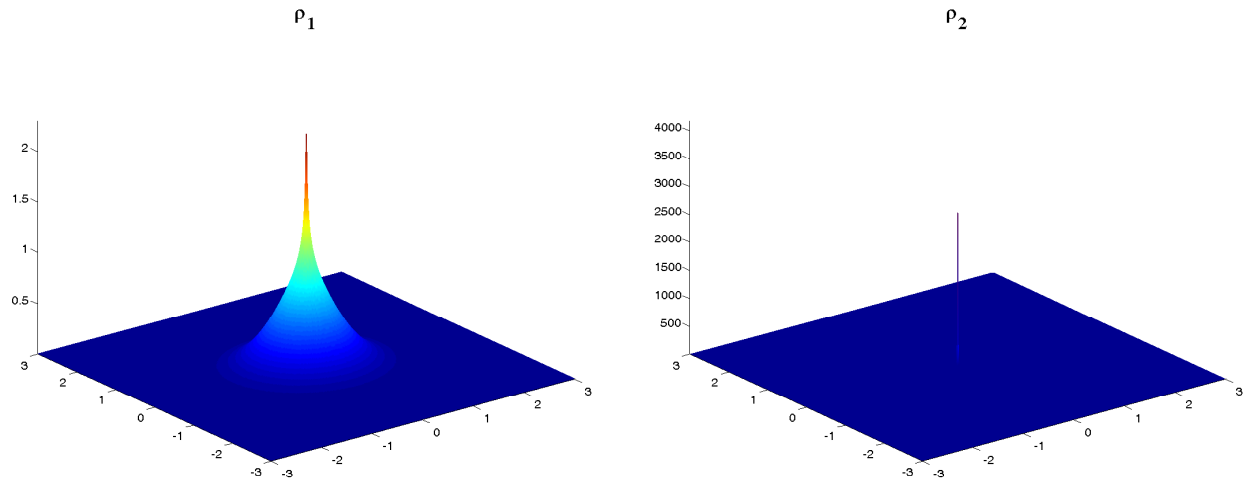

Figure 4.5: Example 3: ρ_1 and ρ_2 at time $t = 0.15$, computed on the 400×400 uniform mesh.

conjecture that non-radially symmetric initial data from Region **B** lead to the same different types of blow-up as in the radially symmetric case.

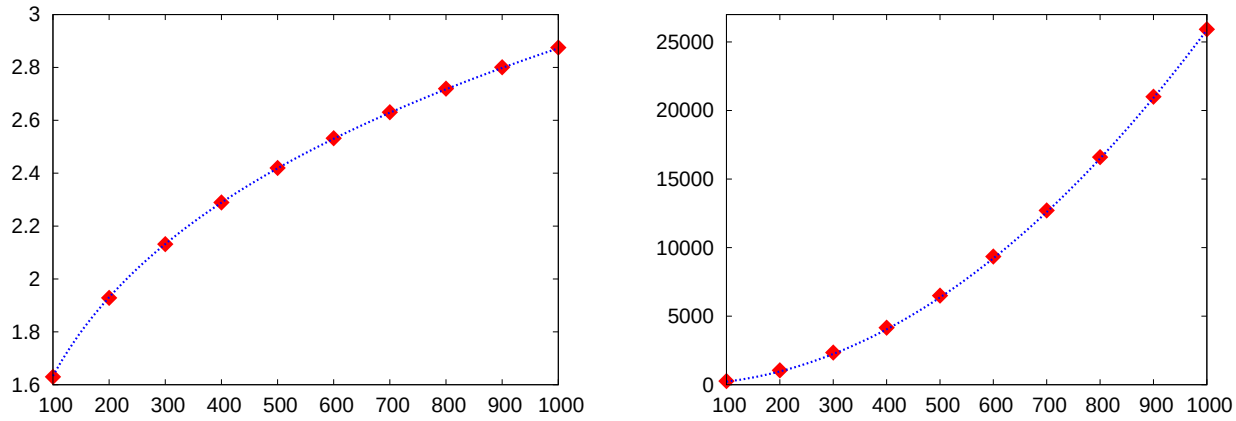

Figure 4.6: Example 3: $\max\limits_{(x,y)\in\Omega} \rho_1(x,y,0.15)$ together with $\eta_1(N) = 0.429(2N+10)^{1/4}$ (left) and $\max\limits_{(x,y)\in\Omega} \rho_2(x,y,0.15)$ together with $\eta_2(N) = 0.0263(N-8)^2$ (right) as functions of N.

Example 4: ρ_2 Blows Up Faster than ρ_1 in Region C. Next, we consider the system (1.2) with $\chi_1 = 6$, $\chi_2 = 100$, $\mu_1 = 1$, and subject to the following initial data:

$$\rho_1(x,y,0) = 10\,e^{-100(x^2+y^2)}, \qquad \rho_2(x,y,0) = 90\,e^{-100(x^2+y^2)}.$$

Figure 4.7 shows that both ρ_2 and ρ_1 blow up, while c stays bounded. One can also observe that ρ_2 seems to blow up faster than ρ_1. To verify this, we perform the mesh refinement study and plot the results obtained on the 200×200 and 400×400 uniform grids at the same time $t = 0.007$. As one can see, the magnitude of ρ_2 increases by a factor of about 4 (from $8.9258 \cdot 10^3$ to $3.2590 \cdot 10^4$),

which clearly indicates that by this time ρ_2 has already blown up. At the same time, ρ_1 increases only by a factor of about 2 (from 55.9119 to 105.1929), which means that ρ_1 is going to blow up a little later. Notice that this numerical experiment confirms the analytical result from [4, 5, 7].

Remark 4.1 We have conducted more numerical experiments (not reported here for the sake of brevity) that confirm the analytical results from [4, 7]: global existence of the solution in Region **A** as well as simultaneous blow-up in Region **D**.

4.1.2 The Regularized System (4.1)

Example 5: Region B, Regularized Solution. We now consider the system (4.1), (1.5) with $s_1^* = s_2^* = 20$ and the same data as in Example 2. A mesh refinement study presented in Figure 4.8 clearly demonstrates that saturated chemotaxis flux prevents blow-up of ρ_2 though a spiky structure is developed.

Example 6: Region C, Regularized Solution. Here, we consider the regularized system (4.1), (1.5) with $s_1^* = s_2^* = 20$ and the same data as in Example 4. The obtained solution is shown in Figure 4.9, where one can see a spiky structure in both density components. Note that while the magnitude of ρ_2 has increased, the magnitude of ρ_1 has slightly decreased. A mesh refinement study (not presented here for the sake of brevity) indicates that unlike the solution of the original system (1.2) (shown in Example 4), the solution of the regularized system (4.1) does not blow up. Moreover, by the time $t = 0.05$ the regularized solution has already reached its (numerical) steady state.

4.2 Parabolic Systems

In this section, we numerically study behavior of solutions of the parabolic system (1.1) and its two regularizations (1.3) and (1.6). In the parabolic case, no analytical results that could have split the (θ_1, θ_2)-plane into particular regions (as it has been done in the parabolic-elliptic case in Section 4.1) are available. However, one can expect the solutions of the parabolic system to behave rather similarly to the solutions of the parabolic-elliptic systems, especially when μ_1/D and μ_2/D are small (in all of our numerical experiments, we take $\mu_1 = \mu_2 = 1$ and $D = 10$).

As in Section 4.1, we perform the numerical experiments on a large square domain (either $[-1.5, 1.5] \times [-1.5, 1.5]$ or $[-3, 3] \times [-3, 3]$ or $[0, 10] \times [0, 10]$) and use the Neumann boundary conditions.

4.2.1 The Original System (1.1)

Example 7: Global Existence. We first consider the system (1.1) with $\chi_1 = 1$, $\chi_2 = 5$, and subject to the following initial data:

$$\rho_1(x, y, 0) \equiv \rho_2(x, y, 0) = 500\, e^{-100(x^2+y^2)}, \quad c(x, y, 0) \equiv 1. \tag{4.4}$$

Our numerical experiments suggest that the solution of this IBVP remains smooth and bounded, and the magnitude of both ρ_1 and ρ_2 monotonically decays in time. A snapshot of the computed solution at time $t = 0.01$ is plotted in Figure 4.10.

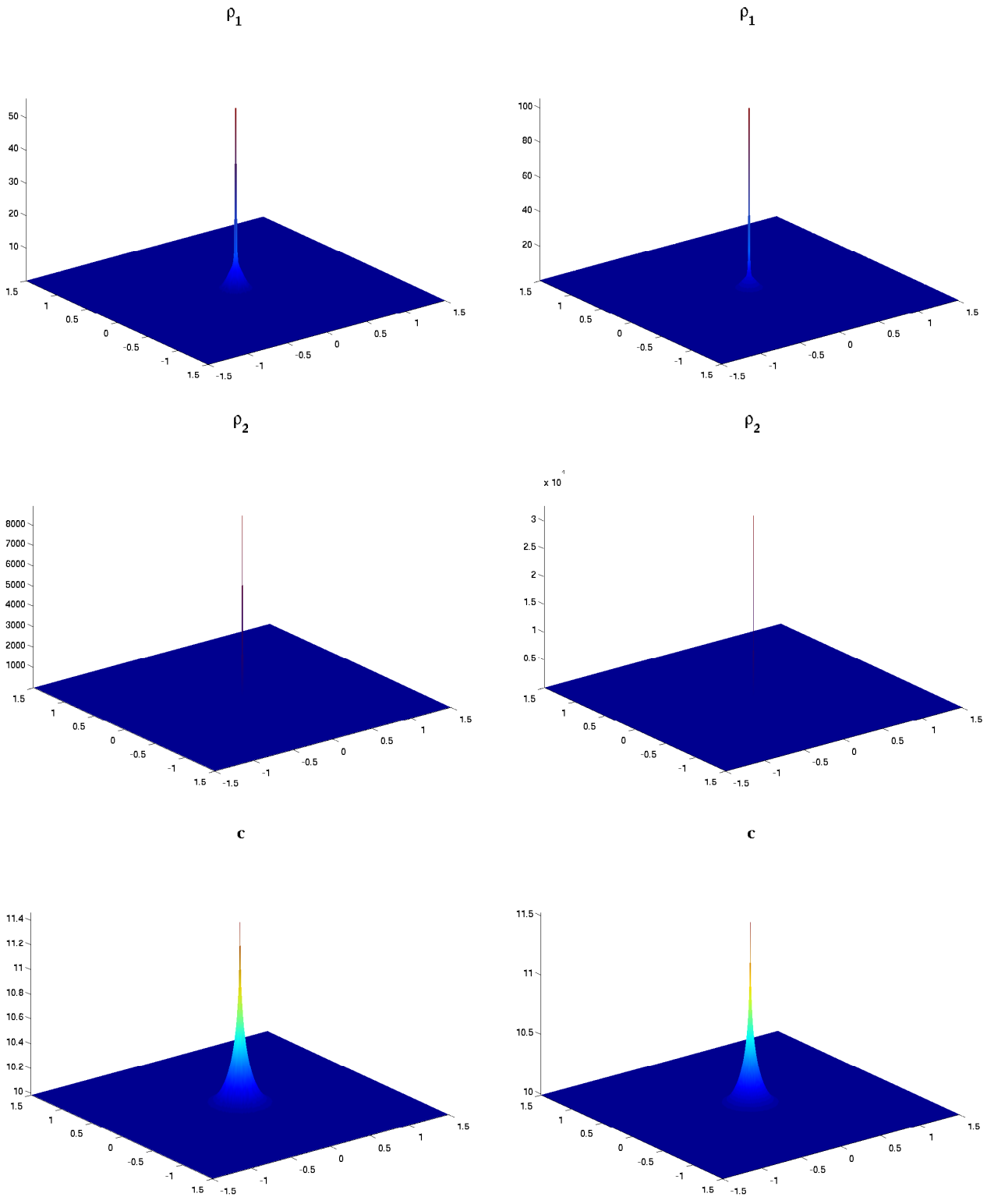

Figure 4.7: Example 4: ρ_1, ρ_2 and c at time $t = 0.007$, computed on the 200×200 (left) and 400×400 (right) uniform meshes.

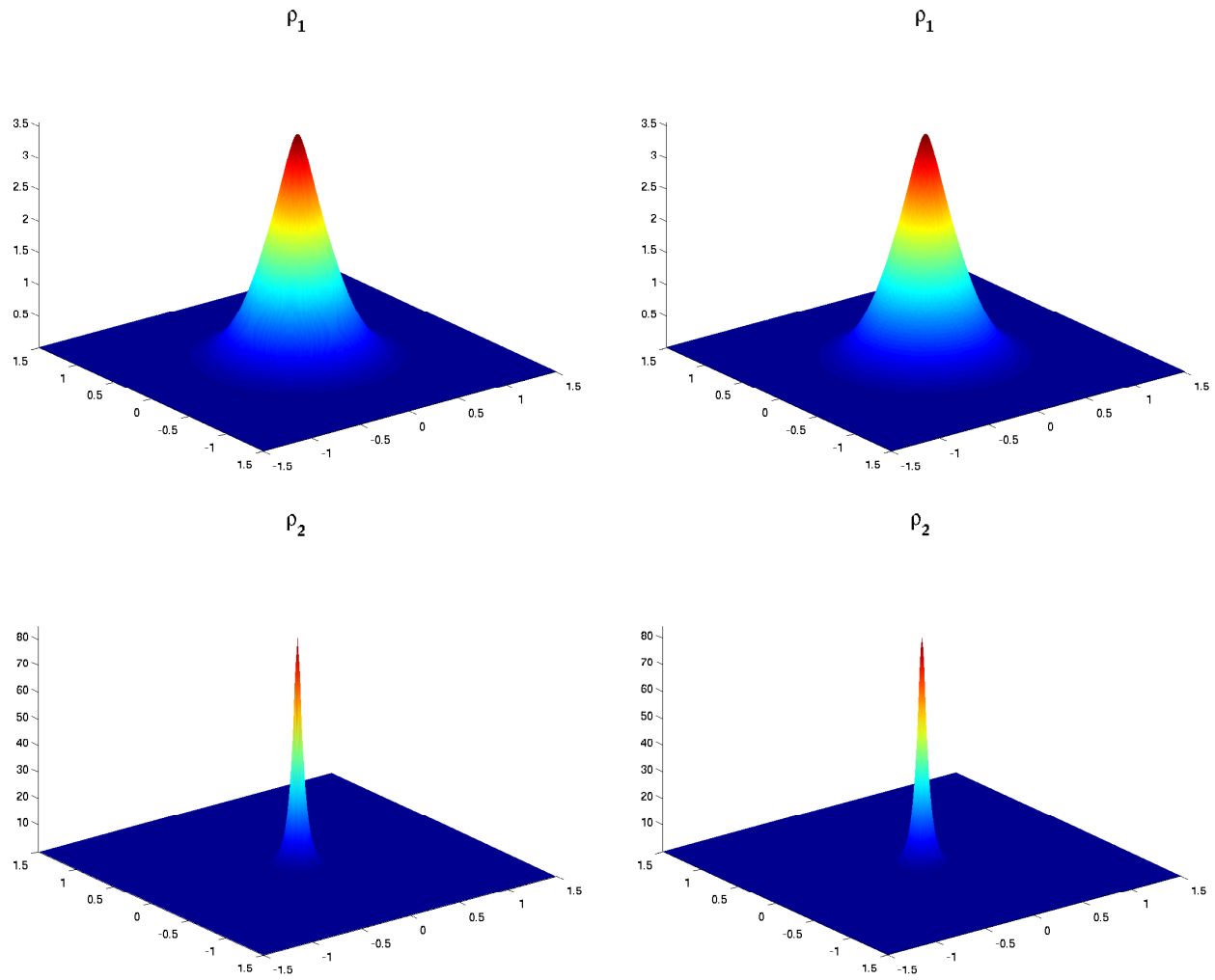

Figure 4.8: Example 5: ρ_1 and ρ_2 at time $t = 0.05$, computed on the 200×200 (left) and 400×400 (right) uniform meshes.

We then double the chemotactic sensitivity of the second species and take $\chi_2 = 10$. This leads to the nonmonotone behavior of ρ_2: Its magnitude first increases, but then starts decreasing and by time $t = 0.05$ (see Figure 4.11) the solution looks similar to the one obtained with $\chi_2 = 5$ (the only difference is that the ratio between the maximum values of ρ_2 and ρ_1 is now about 3 times larger.

Example 8: ρ_2 Blows Up Faster than ρ_1. Next, we consider the system (1.1) subject to the same initial data (4.4), but with much larger chemotactic sensitivity constants $\chi_1 = 5$ and $\chi_2 = 60$. Figure 4.12 shows that both ρ_2 and ρ_1 blow up, but ρ_2 blows up faster than ρ_1 as it is confirmed by the performed mesh refinement study. As one can see, when the mesh size is doubled, the magnitude of ρ_2 increases by a factor of about 4 (from $4.5158 \cdot 10^4$ to $1.8027 \cdot 10^5$), which clearly indicates that by this time ρ_2 has already blown up. At the same time, ρ_1 increases only by a factor of less than 2 (from $1.5263 \cdot 10^3$ to $2.8660 \cdot 10^3$), which means that ρ_1 is going to blow up a little later.

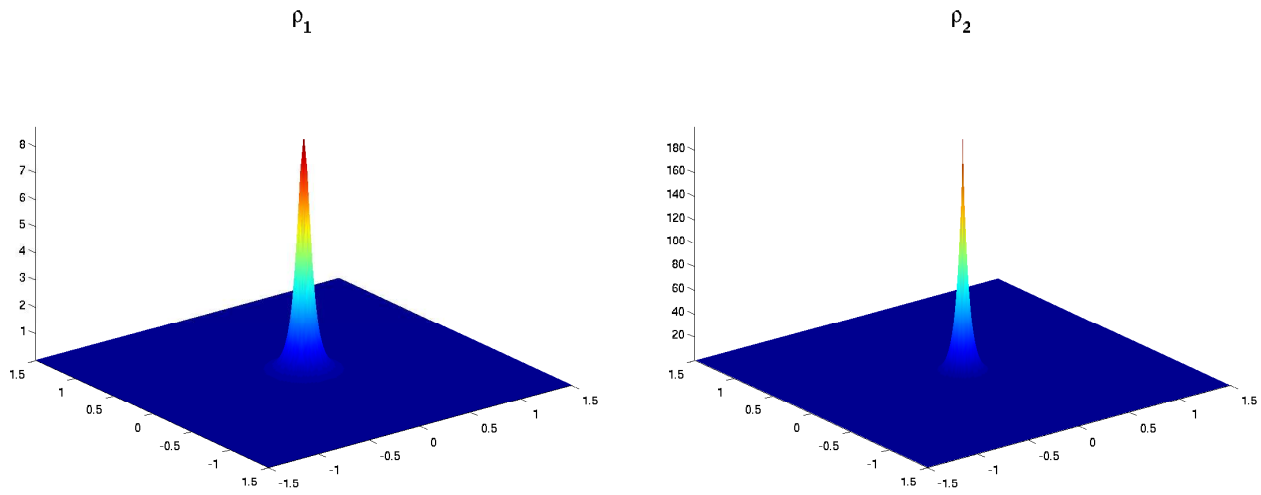

Figure 4.9: Example 6: ρ_1 and ρ_2 at time $t = 0.05$, computed on the 200×200 uniform mesh.

Example 9: Blow-Up of Large Initial Data. In this example, we take much larger initial data,

$$\rho_1(x,y,0) \equiv \rho_2(x,y,0) = 5000\, e^{-100(x^2+y^2)}, \quad c(x,y,0) \equiv 1, \tag{4.5}$$

and the same chemotactic sensitivity constants $\chi_1 = 5$ and $\chi_2 = 60$. As it can be seen in Figure 4.13, both ρ_1 and ρ_2 blow up now much faster than in Example 8.

4.2.2 The Regularized Systems (1.3) and (1.6)

Example 10: Spiky Solutions—No Blowup. We now study the behavior of the solutions of the regularized systems (1.3) and (1.6) subject to the same initial data (4.5) as in Example 9. We first compute the solution of the system (1.3), (1.5) with $s_1^* = s_2^* = 20$. As one can see in Figure 4.14, both ρ_1 and ρ_2 increase and the spikes are formed (notice that they have about the same magnitude even though χ_2 is much larger than χ_1: this is an effect of the regularization). However, the mesh refinement study clearly demonstrates that the solution has not blown up. Our further numerical studies indicate that the obtained spiky solution is a steady state: it does not change as the time increases.

The solution of the second regularized system (1.6) with $\kappa = 0.01$ is shown in Figure 4.15. As one can clearly see, this regularized solution does not blow up as well. However, it behaves differently: by the time $t = 0.01$, $\max_\Omega \rho_2$ has increased, while $\max_\Omega \rho_1$ has decreased. As in the previous case, the obtained solution is a numerical steady state.

We finally decrease the regularization parameter and take $\kappa = 0.001$. The obtained solution, plotted in Figure 4.16, is spiky, but bounded. Notice that now both ρ_1 and ρ_2 increase, but $\max_\Omega \rho_2$ is still about 5 times larger than $\max_\Omega \rho_1$.

Example 11: Multi-Spiky Solutions. In the last example, we take noisy initial data,

$$\rho_1(x,y,0) \equiv \rho_2(x,y,0) = 10(1+\sigma), \quad c(x,y,0) \equiv 1, \tag{4.6}$$

where σ is a random variable uniformly distributed on $[0,1]$. The solutions of both the first regularized system (1.3), (1.5) with $s_1^* = s_2^* = 20$ (see Figure 4.17, left) and the second regularized

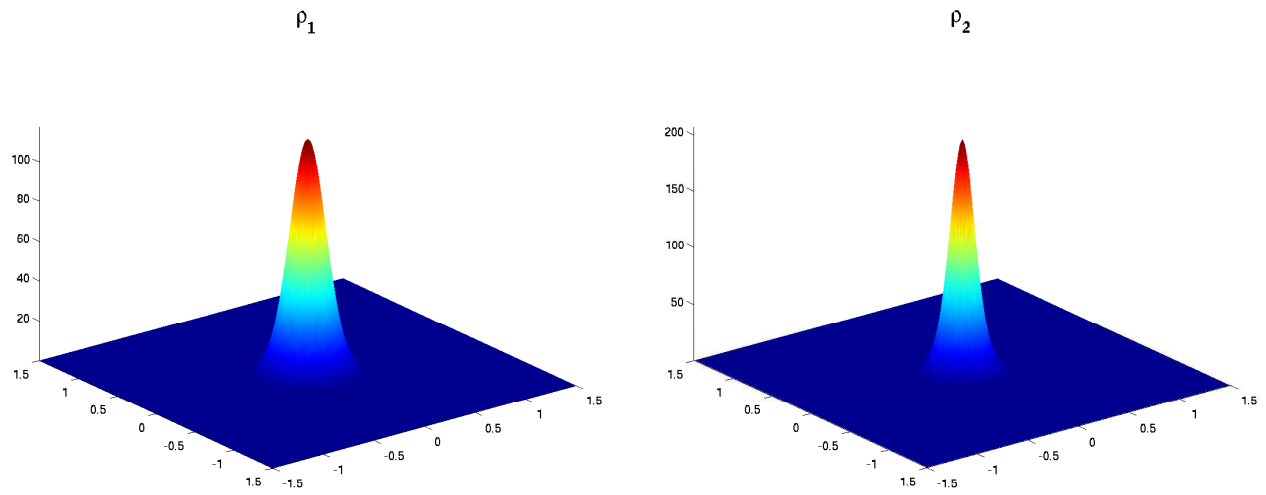

Figure 4.10: Example 7: ρ_1 and ρ_2 at time $t = 0.01$, computed for $\chi_1 = 1$, $\chi_2 = 5$ in the domain $[-1.5, 1.5] \times [-1.5, 1.5]$ using the 200×200 uniform mesh.

system (1.6) with $\kappa = 0.01$ (see Figure 4.17, right) develop a complicated multi-spiky structures. In both cases, the multi-spiky solutions are numerical steady states.

5 Conclusions

In this paper, we have presented a comprehensive numerical study of several two-species chemotaxis Patlak-Keller-Segel type models. We have considered both the parabolic-elliptic as well as the fully parabolic systems. The simplest (yet very challenging for rigorous mathematical analysis) parabolic-elliptic case has been analytically studied in [4, 7]. It has been proven there that under certain conditions on the initial cell densities and chemotactic sensitivity coefficients the system admits global regular solutions, while under a different set of conditions the densities of both species will simultaneously blow up within a finite time. If none of those conditions is satisfied, the question of global existence vs. finite time blow-up remains open. The aim of the present paper has been to present an extensive numerical study of possible configurations and indicate answers to some open questions posted in [4,7]. More precisely, we have demonstrated that for the parabolic-elliptic system the following 3 scenarios are possible: a global solution may exist, the density of one species may blows up faster than the density of the second species, both densities may blow up simultaneously.

In the fully parabolic case, the situation is more complicated and a complete identification of the corresponding conditions for the initial data and parameters is not yet available. Nevertheless, we have demonstrated that the same 3 scenarios are still possible.

Since blow up of the solution can be viewed as a purely mathematical artifact of the classical Patlak-Keller-Segel type models, we have also studied two different regularizations that yield spiky but bounded solutions. We have derived a-priori estimates that confirm that the solutions of the regularized system indeed remain bounded. We have also conducted a number of numerical experiments to study behavior of the obtained spiky solutions.

Acknowledgment: The work of A. Kurganov was supported in part by the German Research

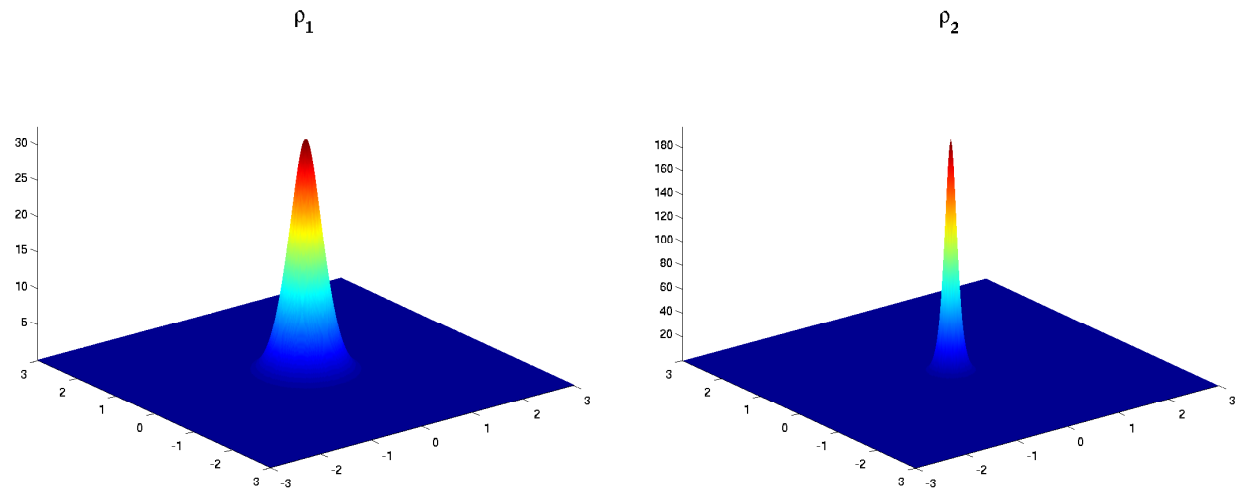

Figure 4.11: Example 7: ρ_1 and ρ_2 at time $t = 0.05$, computed for $\chi_1 = 1$, $\chi_2 = 10$ in the domain $[-3, 3] \times [-3, 3]$ using the 400×400 uniform mesh.

Foundation DFG under the grant # INST 247/609-1 and by the NSF grant # DMS-1115718. The main part of the research was conducted during the Summer of 2011, when the first authors visited the Institute of Mathematics, University of Mainz. The first author would like to thank the faculty and staff for their support and hospitality.

References

[1] A. Chertock, Y. Epshteyn and A. Kurganov, High-order finite-difference and finite-volume methods for chemotaxis models, in preparation.

[2] A. Chertock, A. Kurganov, X. Wang and Y. Wu, On a chemotaxis model with saturated chemotactic flux, *Kinet. Relat. Models*, **5** (2012), 51–95.

[3] S. Childress and J. K. Percus, Nonlinear aspects of chemotaxis, *Math. Biosc.*, **56** (1981), 217–237.

[4] C. Conca, E. Espejo and K. Vilches, Remarks on the blowup and global existence for a two species chemotactic Keller-Segel system in $\mathbb{R}^2$, *European J. Appl. Math.*, **22** (2011), 553–580.

[5] E. E. Espejo, A. Stevens and T. Suzuki, Simultaneous blowup and mass separation during collapse in an interacting system of chemotactic species, *Differential Integral Equations*, **25** (2012), 251–288.

[6] E. E. Espejo, A. Stevens and J. J. L. Velázquez, A note on non-simultaneous blow-up for a drift-diffusion model, *Differential Integral Equations*, **23** (2010), 451–462.

[7] E. E. Espejo, K. Vilches and C. Conca, Sharp condition for blow-up and global existence in a two species chemotactic Keller-Segel system in $\mathbb{R}^2$, *European J. Appl. Math.*, **24** (2013), 297–313.

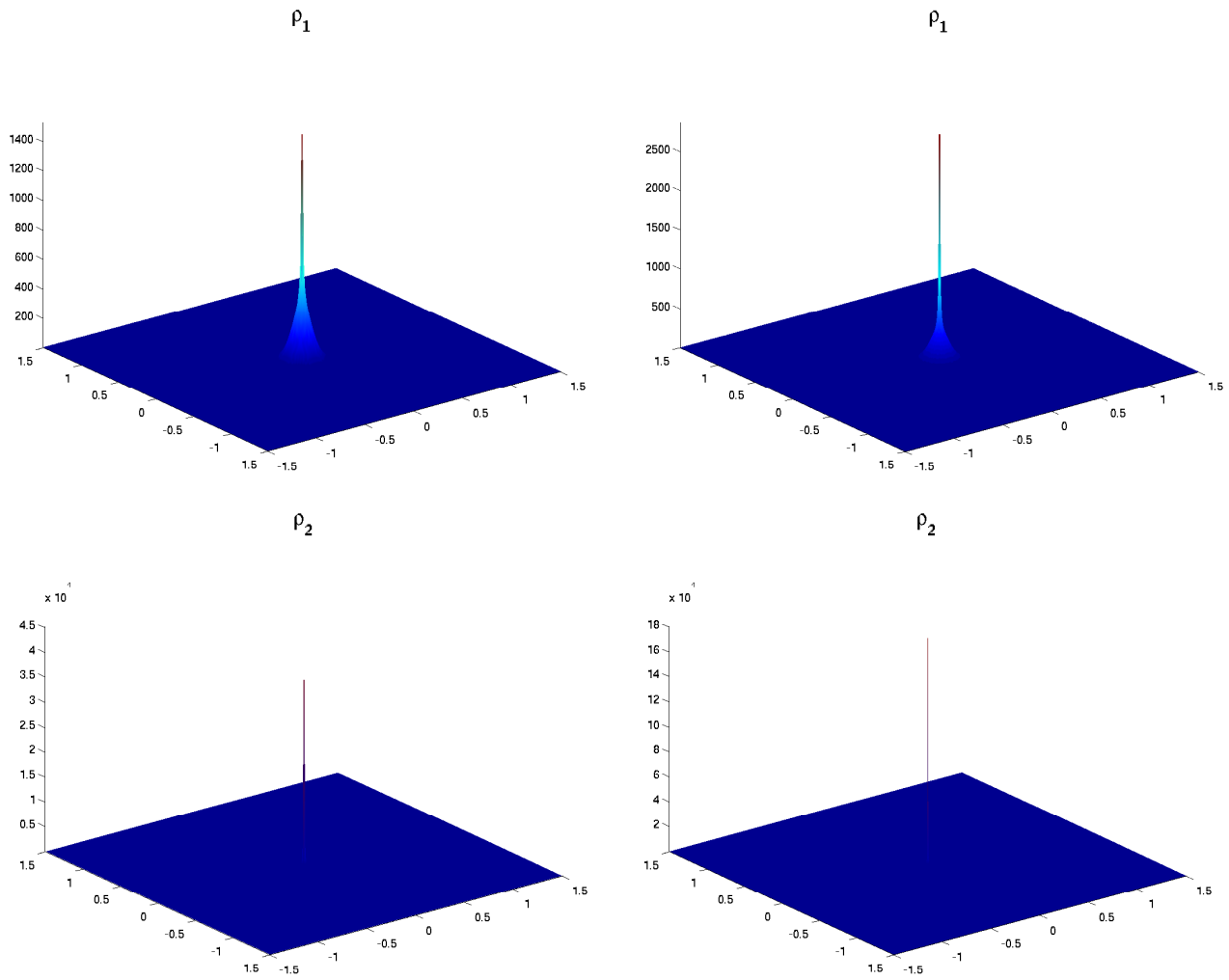

Figure 4.12: Example 8: ρ_1, ρ_2 at time $t = 0.001$, computed on the 200×200 (left) and 400×400 (right) uniform meshes.

[8] E. E. Espejo Arenas, A. Stevens and J. J. L. Velázquez, Simultaneous finite time blow-up in a two-species model for chemotaxis, *Analysis (Munich)*, **29** (2009), 317–338.

[9] A. Fasano, A. Mancini and M. Primicerio, Equilibrium of two populations subject to chemotaxis, *Math. Models Methods Appl. Sci.*, **14** (2004), 503–533.

[10] S. Gottlieb, C.-W. Shu and E. Tadmor, Strong stability-preserving high-order time discretization methods, *SIAM Rev.*, **43** (2001), 89–112.

[11] M. A. Herrero and J. J. L. Velázquez, A blow-up mechanism for a chemotaxis model, *Ann. Scuola Normale Superiore*, **24** (1997), 633–683.

[12] I. Higueras, Characterizing strong stability preserving additive Runge-Kutta methods, *J. Sci. Comput.*, **39** (2009), 115–128.

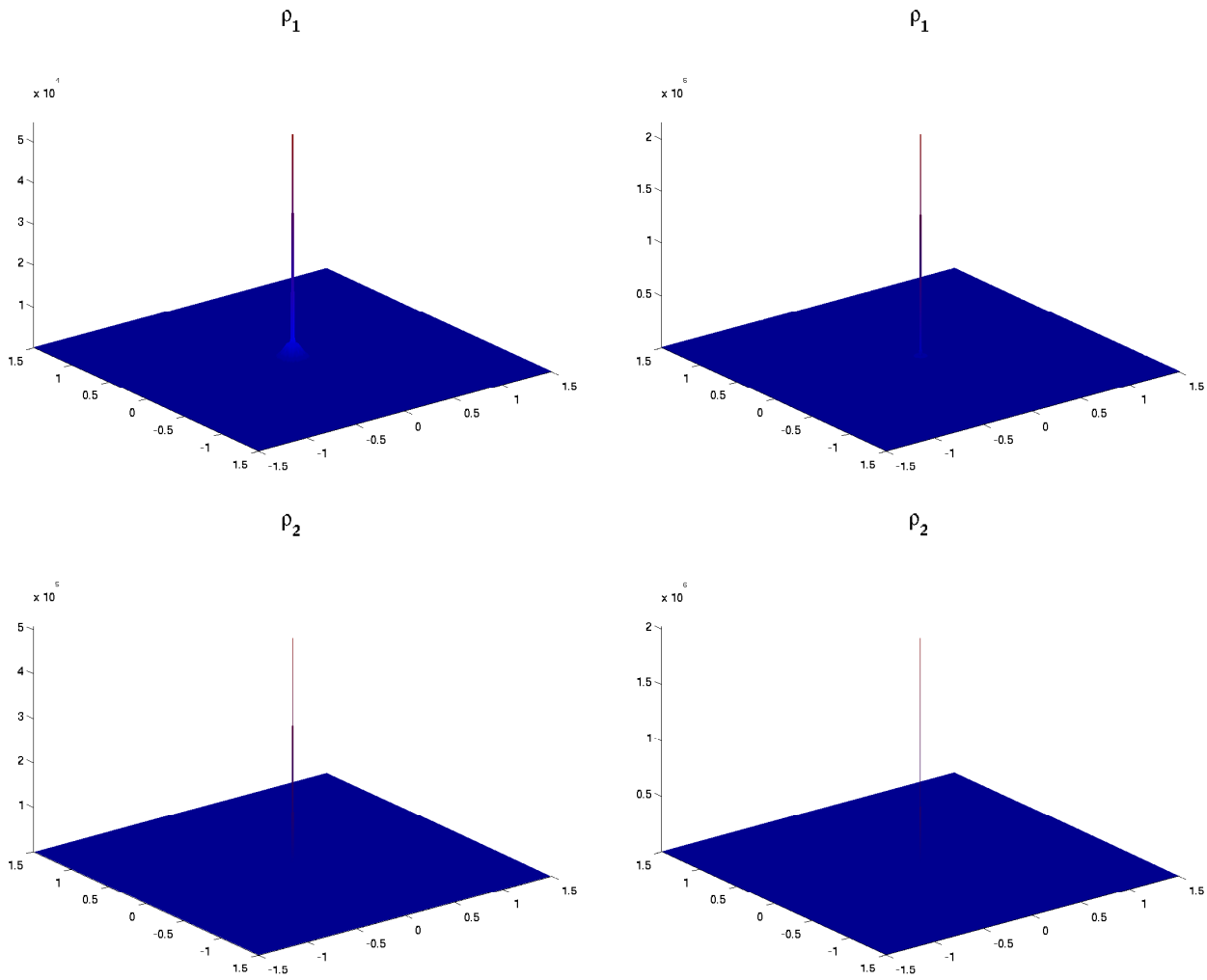

Figure 4.13: Example 9: ρ_1 and ρ_2 at time $t = 0.0002$, computed on the 200×200 (left) and 400×400 (right) uniform meshes.

[13] T. Hillen and K. Painter, Global existence for a parabolic chemotaxis model with prevention of overcrowding, *Adv. in Appl. Math.*, **26** (2001), 280–301.

[14] T. Hillen and K. J. Painter, A user's guide to PDE models for chemotaxis, *J. Math. Biol.*, **58** (2009), 183–217.

[15] T. Hillen, K. Painter and C. Schmeiser, Global existence for chemotaxis with finite sampling radius, *Discrete Contin. Dyn. Syst. Ser. B*, **7** (2007), 125–144.

[16] D. Horstmann, From 1970 until now: The Keller-Segel model in chemotaxis and its consequences I, *Jahresber. DMV*, **105** (2003), 103–165.

[17] D. Horstmann, From 1970 until now: The Keller-Segel model in chemotaxis and its consequences II, *Jahresber. DMV*, **106** (2004), 51–69.

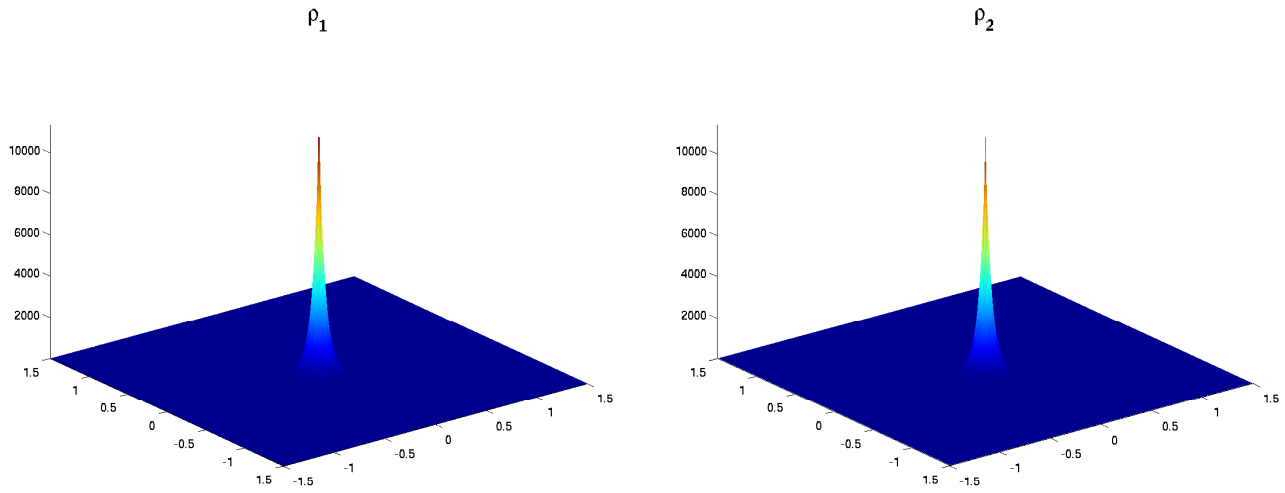

Figure 4.14: Example 10: Solutions (ρ_1 and ρ_2) of (1.3), (1.5), (4.5) with $s_1^* = s_2^* = 20$ at time $t = 0.01$, computed on the 200×200 uniform mesh.

[18] E. F. Keller and L. A. Segel, Initiation of slime mold aggregation viewed as an instability, *J. Theor. Biol.*, **26** (1970), 399–415.

[19] E. F. Keller and L. A. Segel, Model for chemotaxis, *J. Theor. Biol.*, **30** (1971), 225–234.

[20] M. Kurokiba and T. Ogawa, Finite time blow-up of the solution for a nonlinear parabolic equation of drift-diffusion type, *Diff. Integral Eqns.*, **4** (2003), 427–452.

[21] O. A. Ladyženskaja, V. A. Solonnikov and N. N. Ural′ceva, Linear and quasilinear equations of parabolic type, Translated from the Russian by S. Smith, Translations of Mathematical Monographs, **23**, *American Mathematical Society, Providence, R.I.*, (1968).

[22] K.-A. Lie and S. Noelle, On the artificial compression method for second-order nonoscillatory central difference schemes for systems of conservation laws, *SIAM J. Sci. Comput.*, **24** (2003), 1157–1174.

[23] C.-S. Lin, W.-M. Ni and I. Takagi, Large amplitude stationary solutions to a chemotaxis system, *J. Differential Equations*, **72** (1988), 1–27.

[24] T. Nagai, T. Senba and K. Yoshida, Application of the Trudinger-Moser inequality to a parabolic system of chemotaxis, *Funkcial. Ekvac.*, **40** (1997), 411–433.

[25] H. Nessyahu and E. Tadmor, Nonoscillatory central differencing for hyperbolic conservation laws, *J. Comput. Phys.*, **87** (1990), 408–463.

[26] W.-M. Ni, Diffusion, cross-diffusion, and their spike-layer steady states, *Notices Amer. Math. Soc.*, **45** (1998), 9–18.

[27] C. S. Patlak, Random walk with persistence and external bias, *Bull. Math: Biophys.*, **15** (1953), 311–338.

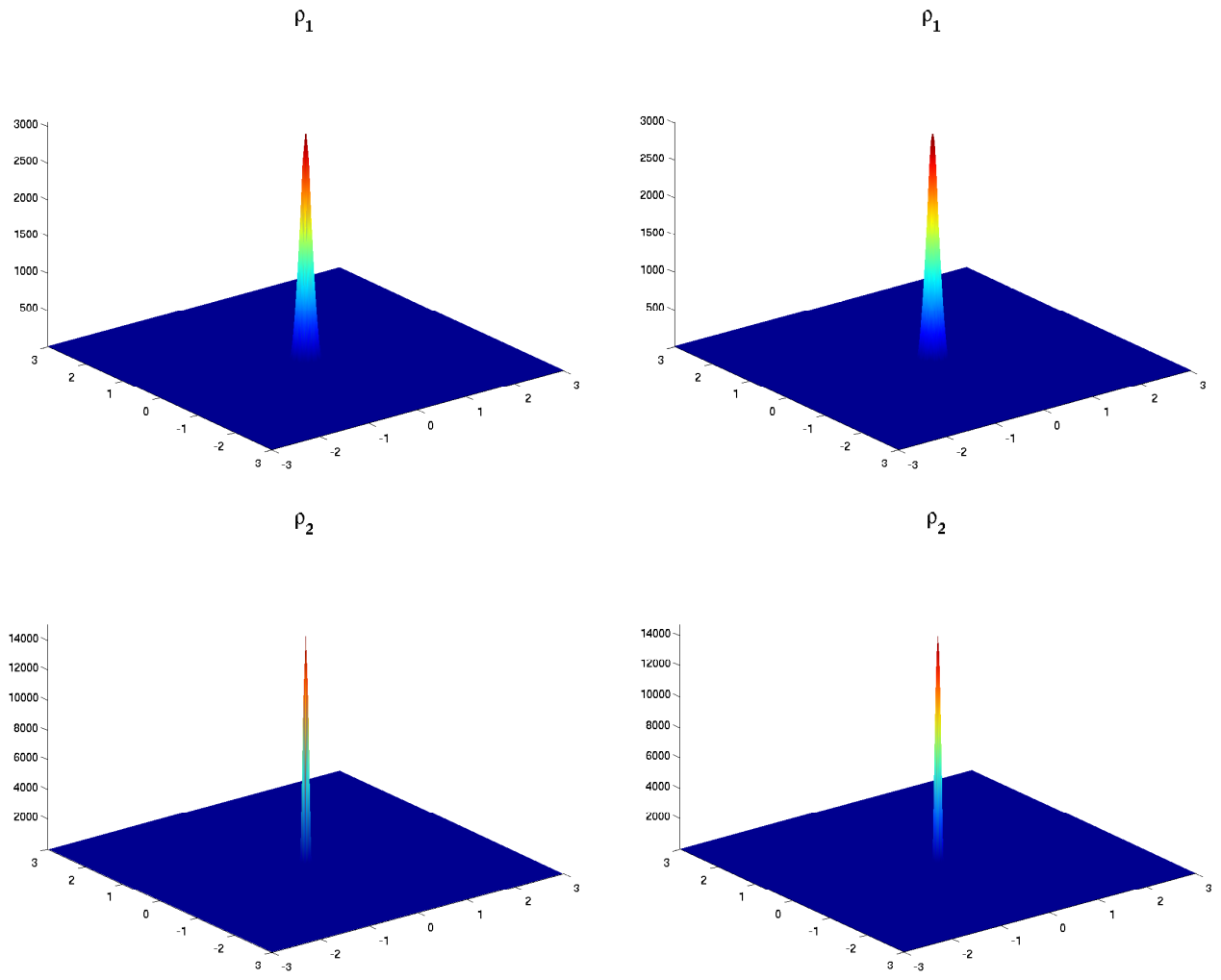

Figure 4.15: Example 10: Solutions (ρ_1 and ρ_2) of (1.6), (4.5) with $\kappa = 0.01$ at time $t = 0.01$, computed on the 400×400 (left) and 800×800 (right) uniform meshes.

[28] B. Perthame, *Transport Equations in Biology*, Frontiers in Mathematics, Birkhäuser Verlag, Basel, 2007.

[29] B. D. Sleeman, M. J. Ward and J. C. Wei, The existence and stability of spike patterns in a chemotaxis model, *SIAM J. Appl. Math.*, **65** (2005), 790–817.

[30] P. K. Sweby, High resolution schemes using flux limiters for hyperbolic conservation laws, *SIAM J. Numer. Anal.*, **21** (1984), 995–1011.

[31] J. J. L. Velázquez, Point dynamics in a singular limit of the Keller-Segel model. I. Motion of the concentration regions, *SIAM J. Appl. Math.*, **64** (2004), 1198–1223.

[32] J. J. L. Velázquez, Point dynamics in a singular limit of the Keller-Segel model. II. Formation of the concentration regions, *SIAM J. Appl. Math.*, **64** (2004), 1224–1248.

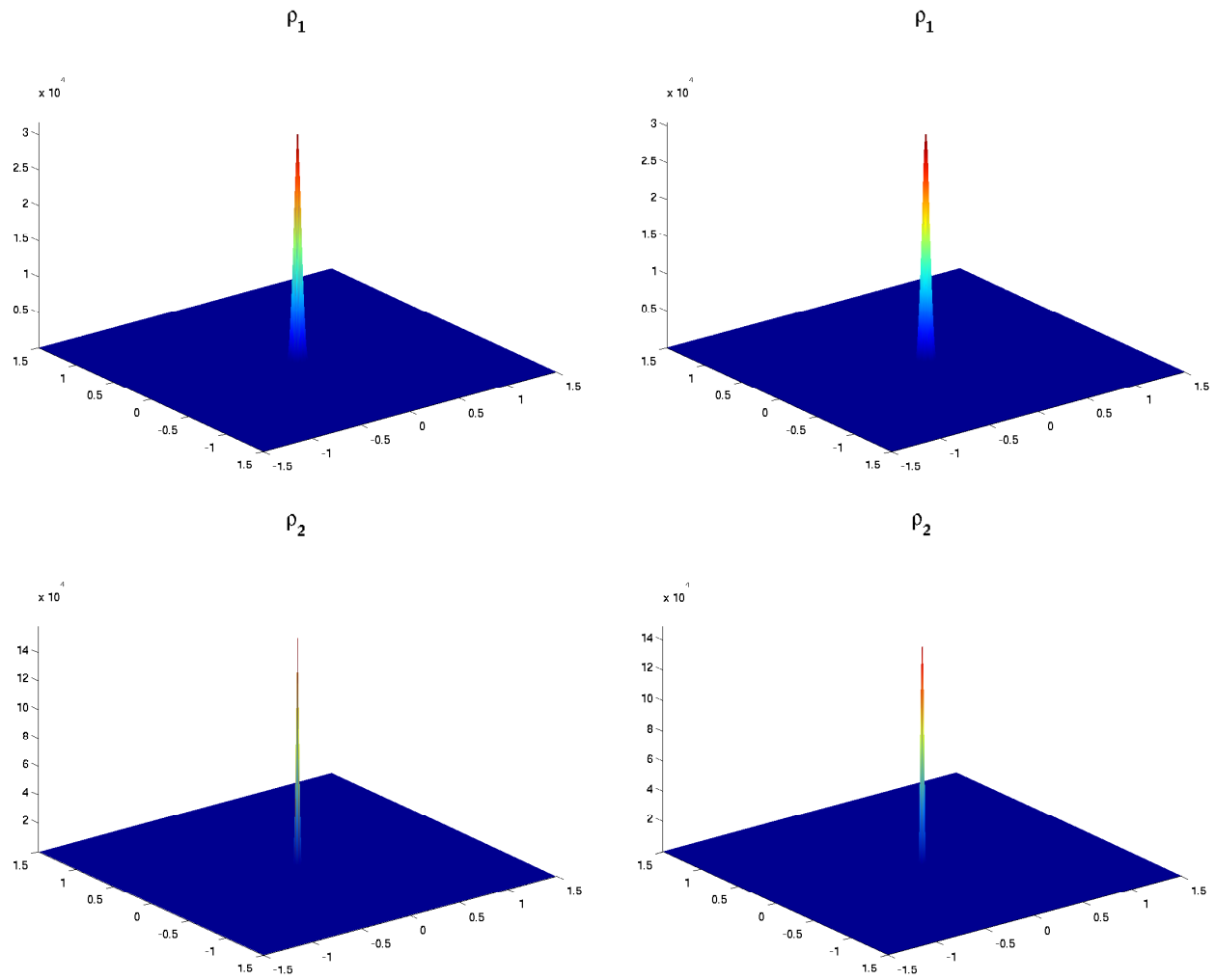

Figure 4.16: Example 10: Solutions (ρ_1 and ρ_2) of (1.6), (4.5) with $\kappa = 0.001$ at time $t = 0.01$, computed on the 200×200 (left) and 400×400 (right) uniform meshes.

[33] X. Wang, Qualitative behavior of solutions of chemotactic diffusion systems: effects of motility and chemotaxis and dynamics, *SIAM J. Math. Anal.*, **31** (2000), 535–560.

[34] G. Wolansky, Multi-components chemotactic system in the absence of conflicts, *European J. Appl. Math.*, **13** (2002), 641–661.

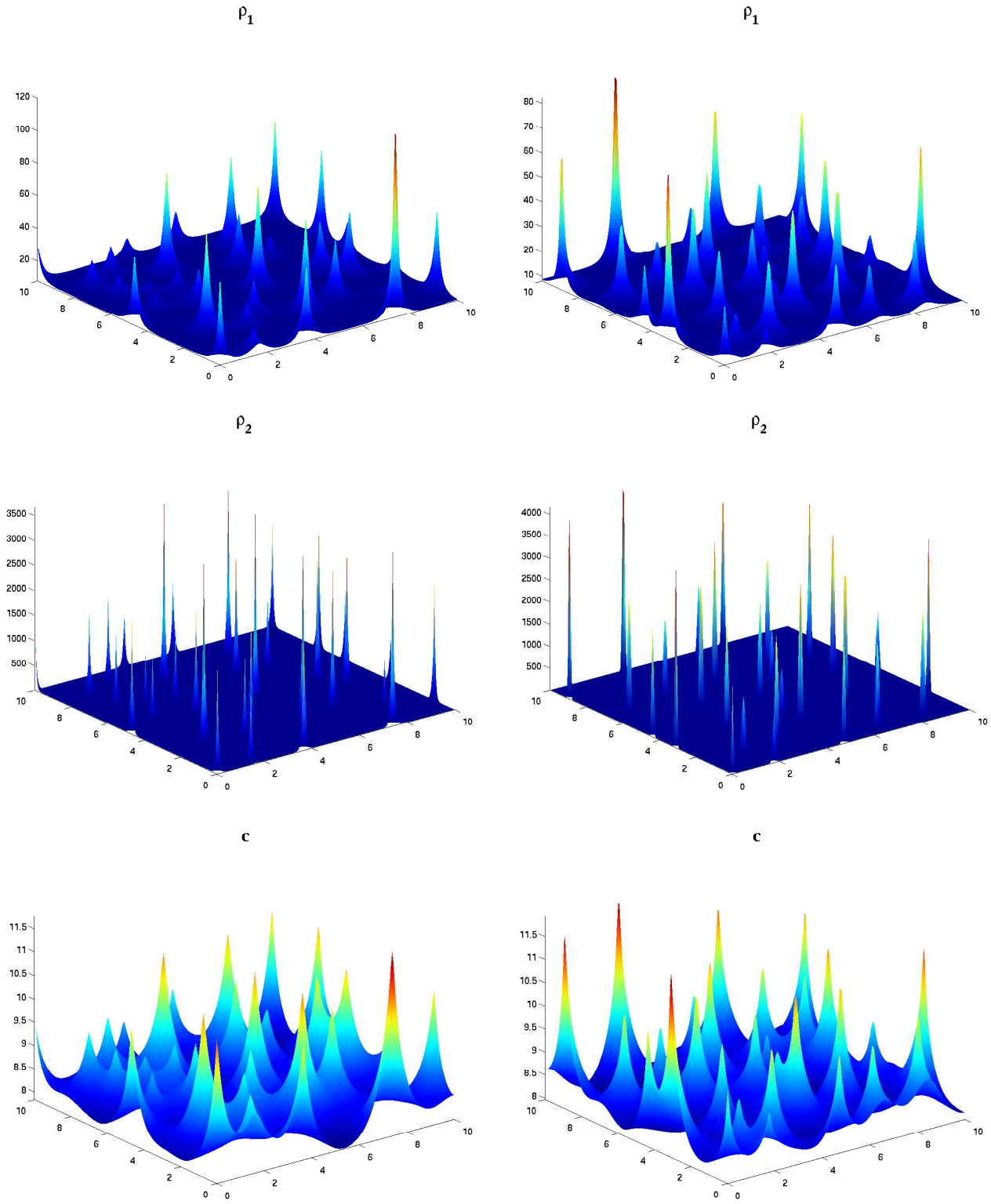

Figure 4.17: Example 11: Solutions (ρ_1, ρ_2 and c) of (1.3), (1.5), (4.6) with $s_1^* = s_2^* = 20$ (left) and of (1.6), (4.6) with $\kappa = 0.01$ (right), computed at time $t = 0.5$ on the 200×200 uniform mesh. $\chi_1 = 5$, $\chi_2 = 60$.